

## Article

# 5-Dodecylsalicylaldoxime as a Novel Collector in Cassiterite Flotation: Performance and Mechanism

Lei Sun <sup>1,2</sup>, Yi Qiao <sup>1,2</sup>, Yang Cao <sup>1,2,\*</sup>, Qingqing Wang <sup>1,2</sup>, Xin Wang <sup>1,2</sup>, Wei Sun <sup>1,2</sup> and Guobin Liu <sup>1,2</sup>

<sup>1</sup> School of Minerals Processing and Bioengineering, Central South University, Changsha 410083, China; sunlei@csu.edu.cn (L.S.); qiaoyi@csu.edu.cn (Y.Q.); wangqingqing@csu.edu.cn (Q.W.); xin.w\_csu@csu.edu.cn (X.W.); sunmenghu@csu.edu.cn (W.S.); liuguobin@csu.edu.cn (G.L.)

<sup>2</sup> Engineering Research Center of Ministry of Education for Carbon Emission Reduction in Metal Resource Exploitation and Utilization, Central South University, Changsha 410083, China

\* Correspondence: caoyang@csu.edu.cn; Tel.: +86-0731-88830482

**Abstract:** Hydroxamic acid and fatty acid collectors are commonly used in cassiterite flotation but face issues like poor selectivity, high dosage, and strict requirements on ore composition and grinding fineness. This study investigates the collecting performance of a novel flotation reagent, 5-dodecylsalicylaldoxime (DSA), in cassiterite flotation. DSA exhibits remarkable selectivity, achieving an impressive 82.5% recovery of Sn at a concentration of only  $9 \times 10^{-5}$  mol/L in single mineral flotation tests. Moreover, DSA significantly outperforms benzohydroxamic acid (BHA), enhancing Sn recovery by 33.55% in artificially mixed ore flotation experiments. In the flotation test of a copper–tin polymetallic ore, compared with the BHA flotation effect, the recovery rate of DSA increased by 12.29% when the Sn grade remained basically unchanged. Analyses such as zeta potential, FT-IR, and XPS indicate that DSA's superior collecting performance stems from its stable adsorption onto cassiterite surfaces through a chelating ring formation, resembling the adsorption mechanism of hydroxamic acid collectors. Furthermore, DSA's larger cluster size in the solution compared to BHA contributes to its enhanced selectivity and collectability. Overall, DSA emerges as a promising alternative to traditional cassiterite flotation collectors, offering a combination of enhanced selectivity, lower dosage requirements, and robustness in complex ore systems.

**Keywords:** cassiterite flotation; 5-dodecylsalicylaldoxime; adsorption mechanism; application



**Citation:** Sun, L.; Qiao, Y.; Cao, Y.; Wang, Q.; Wang, X.; Sun, W.; Liu, G. 5-Dodecylsalicylaldoxime as a Novel Collector in Cassiterite Flotation: Performance and Mechanism. *Minerals* **2024**, *14*, 190. <https://doi.org/10.3390/min14020190>

Academic Editor: Dave Deglon

Received: 20 December 2023

Revised: 2 February 2024

Accepted: 8 February 2024

Published: 11 February 2024



**Copyright:** © 2024 by the authors. Licensee MDPI, Basel, Switzerland. This article is an open access article distributed under the terms and conditions of the Creative Commons Attribution (CC BY) license (<https://creativecommons.org/licenses/by/4.0/>).

## 1. Introduction

Tin is the most indispensable material in the electronics industry, and its demand is growing due to the expansion of circular energy technologies, such as new energy vehicles [1–3]. However, only a small portion (17%) of tin consumption is met through recycling, making primary ore the major source [4]. Cassiterite, the only economically significant tin-bearing mineral [5,6], is usually separated from other minerals (e.g., quartz, calcite, tourmaline, etc.) through gravity separation due to its higher density of  $6.9 \text{ g/cm}^3$  [7,8]. Additionally, flotation is an important method, particularly effective for fine-grained disseminated cassiterite and polymetallic ores, complementing gravity separation [9–11].

In the flotation process of cassiterite, collectors are essential for successful separation. Over time, the evolution of collectors has progressed from fatty acids to more advanced compounds like alkyl sulfosuccinate, arsenic acid, phosphoric acid, and hydroxamic acid [10,12–15]. Oleic acid and alkyl sulfosuccinate are known for their effective collection properties but lack selectivity due to their long alkyl chains [16–18]. A common fatty acid collector is sodium oleate, which has a good collection performance for calcite and  $\text{Ca}^{2+}$  ion-activated quartz. However, these minerals are often associated with cassiterite, resulting in the poor selectivity of sodium oleate against cassiterite [19,20]. Arsenic and phosphoric acids, while effective for cassiterite recovery, are often prohibited due to their

significant environmental impact [21,22]. Currently, hydroxamic acid, particularly benzohydroxamic acid (BHA), is the most extensively studied and utilized collector [23,24]. Research by Wu et al. demonstrated the effectiveness of BHA in recovering high-grade tin concentrate from low-grade tin slime [25]. The interaction between hydroxamic acid and cassiterite involves the formation of a solid chelating ring with tin atoms [26]. However, challenges arise due to cassiterite's low solubility and the limited availability of active surface sites. To overcome this,  $Pb^{2+}$  ions are introduced to activate the surface, which raises environmental concerns [27,28]. At the same time,  $Pb^{2+}$  ions can activate calcite, causing it to enter the concentrate and affect the concentrate grade [29]. Additionally, BHA's hydrophobic group, consisting of only one benzene ring, forms a soluble chelating product with tin atoms, leading to insufficient hydrophobicity in treated cassiterite [30,31]. An alternative collector, 5-dodecylsalicylaldoxime (DSA), presents potential advantages. Similar to BHA in its hydrophilic group, DSA's hydrophobic group includes a robust alkane chain, known for its effectiveness in copper ion extraction. This suggests that DSA could be a promising collector for cassiterite flotation, potentially offering improved efficiency and environmental compatibility.

This research thoroughly investigated the effectiveness of DSA as an alternative to BHA as the collector for cassiterite in the flotation. The study employed single mineral samples and artificially mixed minerals to evaluate DSA's flotation performance. Zeta potential measurement, Fourier transform infrared spectroscopy (FTIR), and X-ray photoelectron spectroscopy (XPS) were used to investigate the adsorption mechanism of DSA on the cassiterite surface. The mechanism by which DSA enhances the hydrophobicity of cassiterite has been conjectured using hydrophobicity calculation and reagent molecular cluster size measurement. On this basis, DSA was applied to the flotation of copper–tin polymetallic ore, and its adaptability in actual ore was explored.

## 2. Materials and Methods

### 2.1. Materials and Reagents

The mineral samples of cassiterite, calcite, and quartz were obtained from Guangxi Province, China. These samples were manually selected, crushed, finely ground by a ceramic ball mill, and screened to obtain 38–74  $\mu\text{m}$  samples for flotation tests of single minerals and artificially mixed minerals, and 38  $\mu\text{m}$  samples were used for XRD, zeta potential, FTIR, and XPS detection. X-ray diffraction (XRD) analysis (Figure 1) revealed that the samples had no other impurities within the detection limit and met the single mineral flotation test requirements.

Analytically pure reagents were utilized for the flotation tests, including DSA and BHA as collectors and terpineol as a frother. Additionally, 0.1 mol/L hydrochloric acid (HCl) and sodium hydroxide (NaOH) solutions were employed as pH adjustment agents for the flotation pulp. Before adding the DSA into the flotation cell, it was ultrasonically dispersed and emulsified in an ultrasonic cleaner (JM-03D-40, Skymen, Shenzhen, China) with a power of 100 W and a frequency of 40 KHz for 10 min to ensure thorough mixing. Throughout the experiments, purity and standardization of test conditions were maintained by consistently using deionized water with a resistivity of  $18 \text{ M}\Omega \times \text{cm}$ . This choice of water was made to ensure the attainment of accurate and reproducible results.

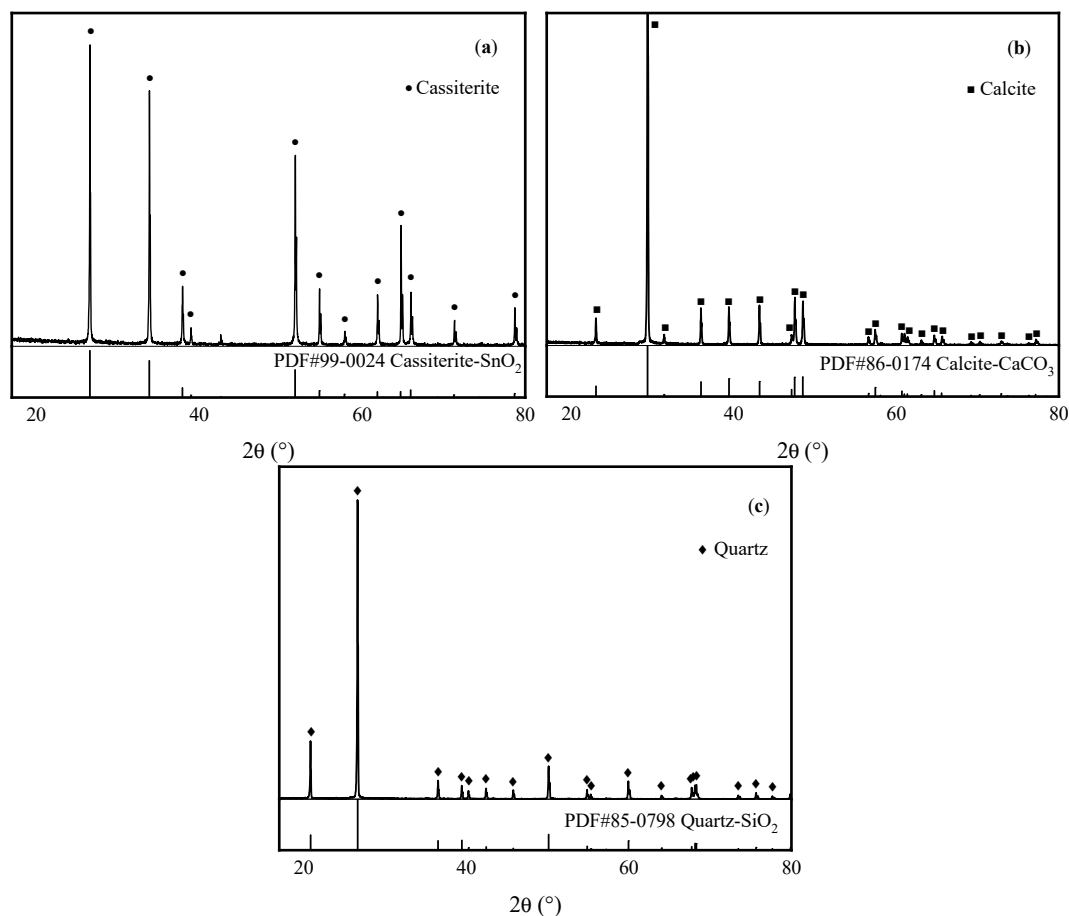


**Figure 1.** XRD pattern of cassiterite (a), calcite (b), and quartz (c) samples.

## 2.2. Methods

### 2.2.1. Micro-Flotation Tests

Micro-flotation experiments were conducted using an XFGII flotation (Jilin Exploration Machinery Plant, Changchun, China) machine equipped with either a 40 mL or 60 mL flotation cell, depending on whether it was a single mineral test or an artificial mixed mineral test. The impeller speed remained constant at 1800 r/min. In each single mineral flotation experiment, 2.0 g of the mineral was dispersed in 35 mL of deionized water at 25 °C, and the pH was adjusted using pH adjusters. After achieving the desired pH level, collector and frother were added and conditioned for 3 min. The flotation process involved manually scraping the foam for 4 min. After the experiment, foam products and tailings were collected, dried, and weighed to calculate mineral recovery.

Artificial mixed mineral flotation tests maintained a 1:1:1 mass ratio of cassiterite, calcite, and quartz, with a procedure closely mirroring the single mineral tests for consistency and meaningful comparisons.

### 2.2.2. Zeta Potential and Reagent Molecules Cluster Size Measurement

In this experiment, the Zetasizer Nano ZS90 (Malvern Panalytical, Shanghai, China) instrument was utilized to measure the zeta potential of cassiterite particles and the size of reagent molecular clusters. Initially, 50 mg of cassiterite particles were well-dispersed in 100 mL of deionized water. Subsequently, pH adjustment was performed, followed by the addition of DSA reagent and a 5 min stirring period. After allowing the suspension to stand for 10 min, an intermediate stable suspension was obtained for measuring the zeta potential of cassiterite particles before and after DSA treatment. The sample preparation steps for measuring reagent molecular cluster size were similar to those mentioned above.

However, it is noteworthy that the suspension concentration used represented the reagent's concentration under optimal conditions for mineral flotation.

### 2.2.3. FTIR Analysis

FTIR analysis was performed using the Nicolet iS50 FTIR Spectrometer (Thermo Fisher Scientific, Waltham, MA, USA). The procedure involved creating a finely ground mixture of cassiterite particles (with a size of approximately 5  $\mu\text{m}$ ) and potassium bromide (KBr) in a mass ratio of 1:100. This mixture was then pressed into a transparent sample sheet for testing. The analysis took place at 25  $^{\circ}\text{C}$  and utilized a mid-infrared light source. To ensure accuracy, temperature and humidity control was maintained in both the sample chamber and the detector. This setup allowed for the measurement of absorption peaks of the flotation agent on the mineral surface, both before and after adsorption. These measurements provided valuable insights into the chemical interactions between the flotation agent and cassiterite, aiding in the understanding of the surface chemistry of the mineral in the context of flotation processes.

### 2.2.4. XPS Analysis

The ESCALAB QXi X-ray photoelectron spectrometer (Thermo Fisher Scientific, Waltham, MA, USA) was used for the X-ray photoelectron spectroscopy (XPS) analysis. The instrument was set to operate at a power of 150 W (15 kV  $\times$  10 mA), a setting that balanced energy efficiency with the precision required for detailed analysis. Specifically, a step size of 1.0 electron volts was chosen for the general XPS spectra, and an even finer resolution of 0.1 electron volts for high-resolution XPS spectra. This precise spectral resolution is crucial for accurately determining binding energies, as it reveals the elemental composition, chemical state, and electronic state of the sample surfaces. The accuracy of the data was further enhanced by using the C1 peak at 284.8 eV, which served to correct the binding energy scale and align the measurements with established reference standards.

## 3. Results and Discussions

### 3.1. Mineral Separation

#### 3.1.1. Micro-Flotation of Single Mineral

This study investigates the flotation recoveries of cassiterite, quartz, and calcite in response to pulp pH changes, using two collectors:  $9 \times 10^{-5}$  mol/L DSA and  $9 \times 10^{-4}$  mol/L BHA. As shown in Figure 2, cassiterite shows a positive correlation with pH levels, reaching a stable recovery of approximately 82.5% between pH 5.6 and 11.0 with DSA, but only 52% with BHA. Calcite, tested only in neutral and alkaline conditions due to its dissolution in acidic environments, exhibits increased recovery in this range, indicating better floatability in alkaline environments. Quartz, conversely, is less sensitive to pH variations, maintaining a low recovery of under 7% across all pH levels. The recovery of cassiterite was higher at a pH of  $8.5 \pm 0.3$ , showing a significant difference compared to calcite and quartz. Consequently, subsequent flotation experiments were conducted under these conditions to favor cassiterite enrichment.

Figure 3 presents the effect of DSA concentration on the flotation recoveries of cassiterite, calcite, and quartz at pH  $8.5 \pm 0.3$ . Cassiterite demonstrates a positive correlation between recovery rate and DSA concentration within the range of  $0$ – $1.4 \times 10^{-4}$  mol/L, peaking at 82% recovery at  $9 \times 10^{-5}$  mol/L. Similarly, calcite also experiences improved recovery with higher DSA concentrations, but its growth is slower, reaching a maximum of 31.5%. In contrast, quartz exhibits minimal variations in recovery across all DSA concentrations, consistently remaining below 7%. These findings indicate that DSA concentration significantly impacts cassiterite and calcite recoveries while having negligible effects on quartz under the specified conditions.

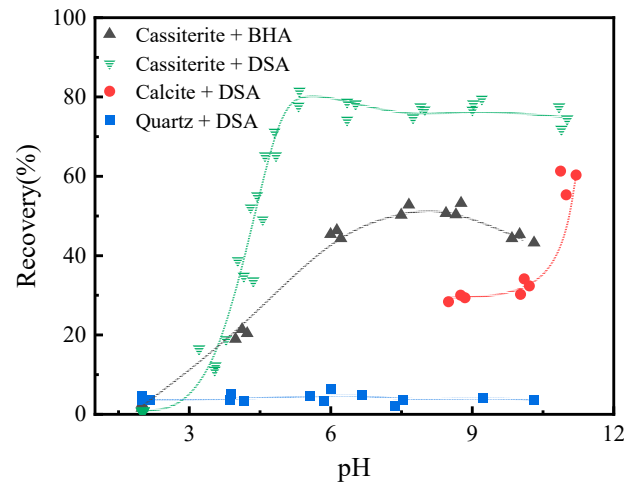


**Figure 2.** Effect of pH on flotation recoveries of cassiterite, calcite, and quartz at  $9 \times 10^{-5}$  mol/L DSA and  $9 \times 10^{-4}$  mol/L BHA.

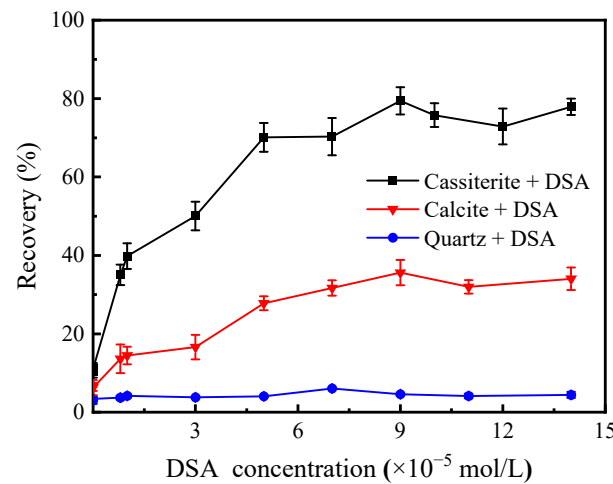


**Figure 3.** Effect of DSA concentration on the flotation recoveries of cassiterite, calcite, and quartz at pH  $8.5 \pm 0.3$ .

### 3.1.2. Micro-Flotation of Artificial Mixed Ore

Mining operations often involve extracting a variety of minerals that are intricately intermixed within a complex mineralogical matrix, posing challenges for the extraction process. Flotation systems designed for mixed minerals provide a more accurate representation of real-world production scenarios compared to those targeting a single mineral. In light of this, the flotation experiments were conducted using artificially mixed minerals to assess the separation efficiency of cassiterite, calcite, and quartz using DSA and BHA as collectors, as shown in Figure 4.

As illustrated in Figure 4, the tin grade exhibits an upward trend with increasing DSA concentration, reaching its peak value of 27.2% at a DSA concentration of  $5 \times 10^{-5}$  mol/L, alongside a tin recovery rate of 60.12%. As the DSA concentration is further increased, tin recovery continues to rise, but the tin grade starts to decline, indicating the flotation of calcite and quartz alongside cassiterite. When employing BHA as a collector, although the trends in tin grade and recovery resemble those of DSA, the tin recovery is considerably lower compared to DSA, even when achieving the same tin grade. Notably, DSA only requires one-tenth of the concentration of BHA for effective separation. For example, at DSA and BHA concentrations of  $7 \times 10^{-5}$  mol/L and  $7 \times 10^{-4}$  mol/L, respectively,

both resulted in a tin grade of 24.2%, but the tin recovery rates were 80.44% and 46.89%, respectively.

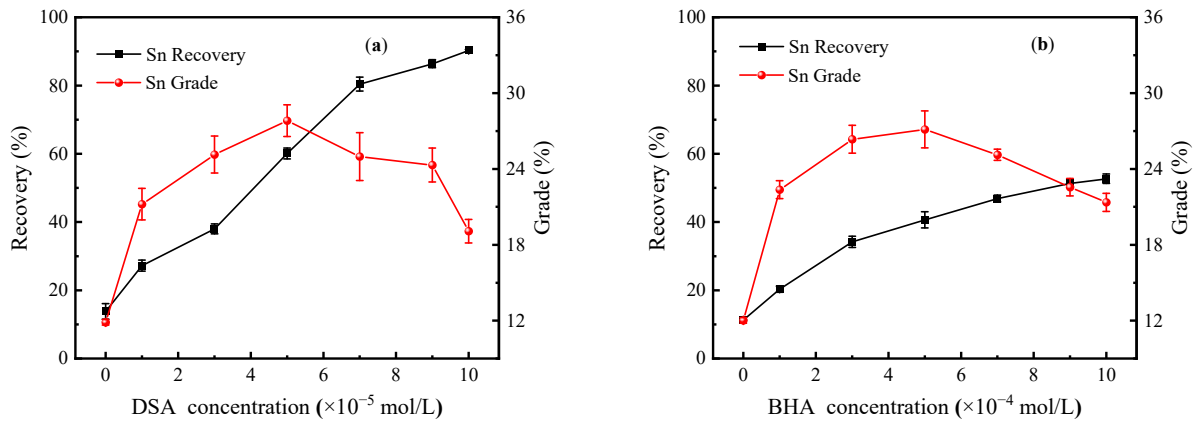


**Figure 4.** Effect of DSA (a) and BHA (b) concentrations on cassiterite flotation recovery in artificially mixed ore at pH  $8.5 \pm 0.3$ .

### 3.2. Mechanism of the Interaction between DSA and Minerals

#### 3.2.1. Zeta Potential Measurements

The zeta potentials of cassiterite, DSA molecular clusters, and DSA-treated cassiterite were measured to elucidate the adsorption mechanism of DSA on the surface of cassiterite, as depicted in Figure 5.

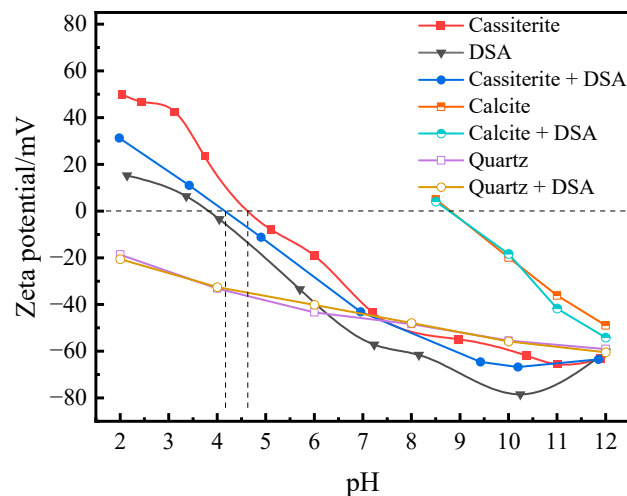


**Figure 5.** The effect of pH on the zeta potential of cassiterite, quartz, and calcite before and after DSA treatment, and DSA molecular clusters.

The isoelectric point (IEP) of natural cassiterite was found to be at a pH of 4.6, which is consistent with prior research [32,33]. For all three substances, zeta potentials are negatively correlated with pH, but their absolute values exhibit a positive correlation with pH beyond their respective IEPs. This trend is especially notable in DSA, where the absolute value of its zeta potential surpasses 30 mV at pH levels above 5.6. This significant increase in DSA’s zeta potential is crucial for its effective dispersion in the pulp, potentially enhancing the flotation efficiency of cassiterite [34]. Furthermore, there is a noticeable shift in the IEP of DSA-treated cassiterite towards lower pH values. This shift is likely attributable to the adsorption of DSA onto the cassiterite surface, altering its surface charge characteristics. However, considering the charge characteristics of cassiterite and DSA, the likelihood of electrostatic interaction between them appears to be minimal. The zeta potential of

calcite undergoes a significant negative shift when the pH exceeds 10, suggesting that DSA exhibits notable adsorption on the surface of calcite. Conversely, the zeta potential of quartz remains largely unchanged after DSA addition. These observations align with the results of single-mineral flotation experiments.

### 3.2.2. FTIR Analysis

This study further explores the adsorption mode of DSA on the cassiterite surface through Fourier-transform infrared (FTIR) analyses. Figure 6 illustrates the FTIR spectrum of cassiterite, DSA-treated cassiterite, and DSA.

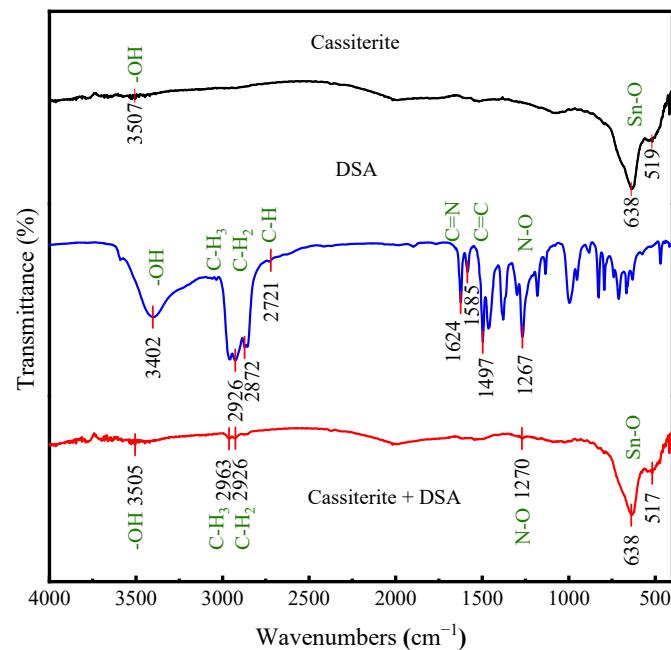


**Figure 6.** FTIR spectra of cassiterite, DSA, and DSA-treated cassiterite.

The IR spectrum of natural cassiterite shows notable peaks at  $638\text{ cm}^{-1}$  and  $519\text{ cm}^{-1}$ , which are attributed to the antisymmetric vibration of the Sn-O bond [25,35]. This indicates the fundamental structural components of the cassiterite. Additionally, a significant peak at  $3507\text{ cm}^{-1}$  is observed, corresponding to the stretching vibration of the hydroxyl group [36]. This peak is linked to the interaction between water molecules and the cassiterite surface, suggesting the presence of adsorbed water or surface hydroxylation. In contrast, the FTIR spectrum of DSA displays characteristic peaks at different frequencies, highlighting the molecular structure of the DSA. Peaks at  $2721\text{ cm}^{-1}$  and  $1624\text{ cm}^{-1}$  represent the stretching vibrations of the C-H and C=N bonds, respectively, which are integral to the oxime group in the DSA molecule. Additionally, peaks observed at  $1497\text{ cm}^{-1}$  and  $1585\text{ cm}^{-1}$  are associated with the vibrations of the C=C bond within the benzene ring belonging to DSA [37,38]. Furthermore, the spectrum of DSA also shows peaks at  $2926\text{ cm}^{-1}$  and  $2872\text{ cm}^{-1}$ , associated with the stretching vibrations of the -CH<sub>3</sub> and -CH<sub>2</sub> groups in alkanes [22,39]. The FTIR analysis of DSA-treated cassiterite reveals notable changes in the vibrational absorption peaks. Specifically, the C-H stretched vibrational absorption peaks, attributed to the dodecyl group on DSA, are observed at  $2926\text{ cm}^{-1}$  and  $2963\text{ cm}^{-1}$ . Additionally, the absorption peak at  $1270\text{ cm}^{-1}$ , representing the N-O stretching vibration in the oxime group, shows a shift from the original peak at  $1267\text{ cm}^{-1}$  [40]. Furthermore, a subtle but significant shift is noted in the absorption peaks of the Sn-O bond in cassiterite, moving from  $638\text{ cm}^{-1}$  and  $519\text{ cm}^{-1}$  in untreated cassiterite to  $638\text{ cm}^{-1}$  and  $517\text{ cm}^{-1}$  in the DSA-treated sample. This shift in the Sn-O bond peaks is indicative of a chemical reaction occurring on the surface of the cassiterite. These spectral changes provide critical

insights into the interactions and chemical alterations induced by DSA on the cassiterite surface.

These spectral changes in the FTIR analysis reveal that DSA treatment alters the surface chemistry of cassiterite. The shifts in vibrational frequencies and the appearance of new peaks suggest chemical bonding or interaction between DSA molecules and the cassiterite surface, leading to changes in the surface properties of the mineral.

### 3.2.3. XPS Analysis

In this study, XPS reveals significant changes in the surface composition of cassiterite following DSA treatment. The XPS survey spectra of natural cassiterite and DSA-treated cassiterite are shown in Figure 7. The XPS survey spectra show that while natural cassiterite lacks a nitrogen core peak, indicating high purity, DSA-treated cassiterite exhibits a noticeable 0.7% N1s concentration and an enhanced carbon (C1s) peak. These changes suggest the successful adsorption of DSA onto the cassiterite surface, a conclusion corroborated by zeta potential and FTIR analyses.

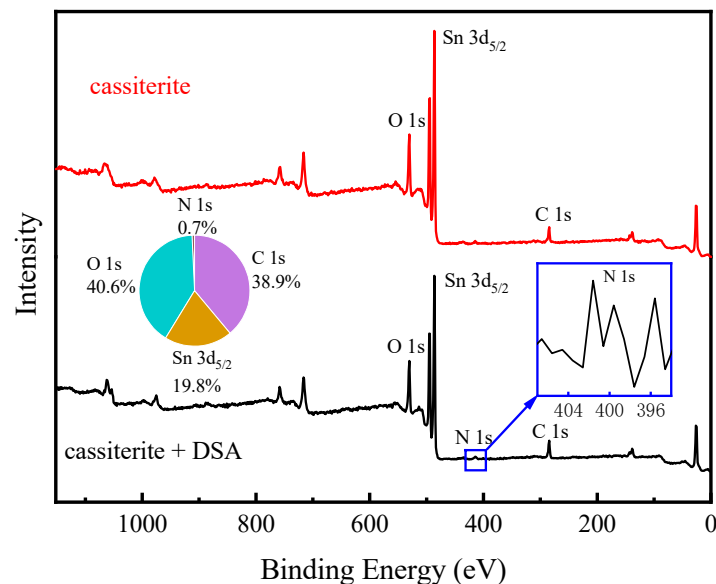


**Figure 7.** XPS spectra of cassiterite with and without DSA.

Figure 8 presents the high-resolution spectra of Sn 3d, O 1s, and N 1s of natural and DSA-treated cassiterite. In natural cassiterite, the binding energies for Sn 3d<sub>3/2</sub> and Sn 3d<sub>5/2</sub> are 495.00 eV and 486.47 eV, respectively, with the difference attributed to spin-orbit coupling [41,42]. After DSA treatment, these binding energies slightly shift to 495.07 eV for Sn 3d<sub>3/2</sub> and 486.62 eV for Sn 3d<sub>5/2</sub>. The shift is caused by the interaction between DSA's highly electronegative O or N atoms and the Sn atoms on the surface of cassiterite. This interaction reduces the electron cloud density around the Sn atoms, which weakens the nuclear electron shielding. This evidence indicates that the Sn atoms on the surface of cassiterite are critical sites for DSA adsorption.

In Figure 8b, the high-resolution O1s spectrum of cassiterite reveals significant changes before and after DSA treatment. Initially, three distinct peaks are observed in the O1s spectrum of natural cassiterite: a low binding energy peak at 530.33 eV for lattice oxygen, a peak at 531.60 eV associated with oxygen vacancies, and the highest binding energy peak at 533.90 eV, which is linked to hydroxylated terminal O atoms on the surface of the cassiterite [43–45]. After the DSA treatment, the peaks for lattice oxygen and oxygen vacancies show negligible change. However, the 533.90 eV peak is observed to vanish, presumably due to the removal of hydroxylation brought about by DSA adsorption. Furthermore, two new peaks emerge at 530.87 eV and 533.15 eV. The peak at 530.87 eV is attributed to the O atom in the C-OH group, whereas the peak at 533.15 eV is linked to the O atom in the

N-OH group. This difference in binding energies is ascribed to the conjugation of benzene rings in DSA. This conjugation increases the electron cloud density around the O atoms in C-OH compared to those in N-OH, leading to a stronger nuclear electron shielding effect and resulting in distinct binding energies for these groups. In Figure 8c, a significant finding is the emergence of a distinct N 1s peak in the DSA-treated cassiterite, indicative of the oxime group. This new peak provides evidence for the adsorption of DSA onto the cassiterite surface. The likely mechanism for this adsorption involves a reaction between the O or N atoms in the DSA molecule and the Sn atoms on the cassiterite surface. This interaction aligns with the previously observed changes in the Sn 3d and O1s spectra, further supporting the idea of chemical modifications on the cassiterite surface due to DSA treatment.

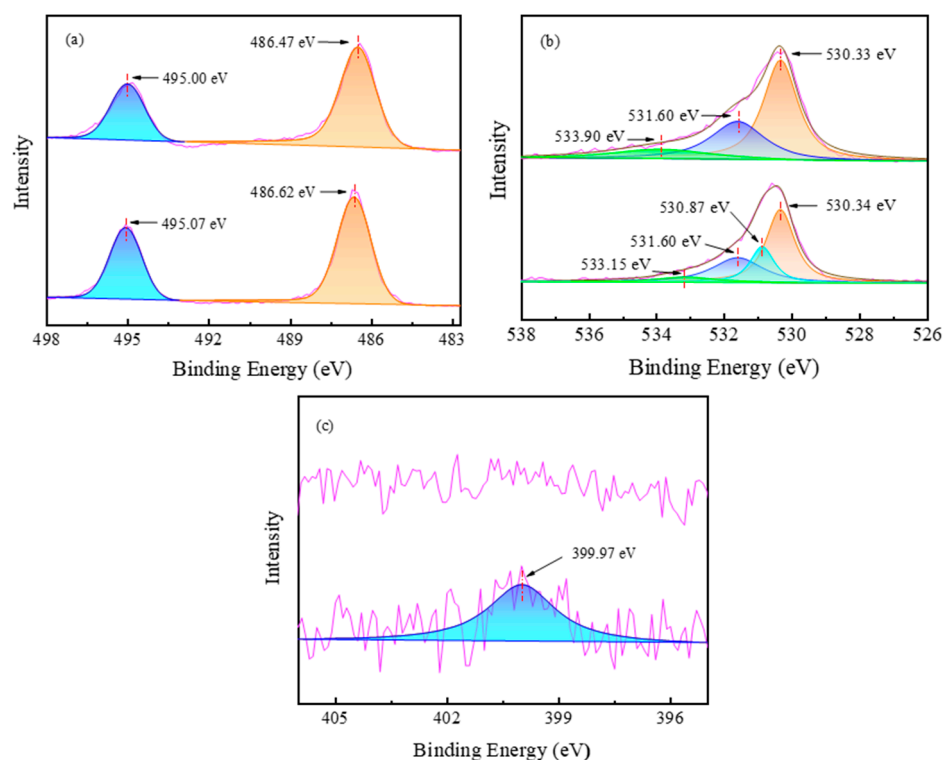


**Figure 8.** High-resolution XPS of Sn 3d (a), O 1s (b), and N 1s (c).

### 3.2.4. Reagent Molecules Cluster Size Measurement

Previous research demonstrated that when DSA and BHA reagents adsorb on the mineral surface, they tend to form clusters rather than exist as individual molecules. This phenomenon is illustrated in Figure 9, which presents the size distribution of clusters generated by DSA and BHA when introduced into deionized water. Notably, the median cluster size (D50 value) for DSA clusters is significantly larger, measuring 3072 nm, compared to BHA clusters with a D50 value of 373 nm. This observation indicates that DSA clusters are significantly larger than those formed by BHA. In addition, DSA has a long alkane chain, which makes it more hydrophobic. This difference in hydrophobicity likely contributes to the formation of larger molecular clusters in solution, possibly through hydrophobic association. When cassiterite surfaces offer equal adsorption sites, DSA exhibits a higher adsorption capacity than BHA. This implies that DSA can more effectively adsorb onto cassiterite surfaces, a characteristic that renders cassiterite treated with DSA more hydrophobic. This increased hydrophobicity is beneficial for flotation recovery.

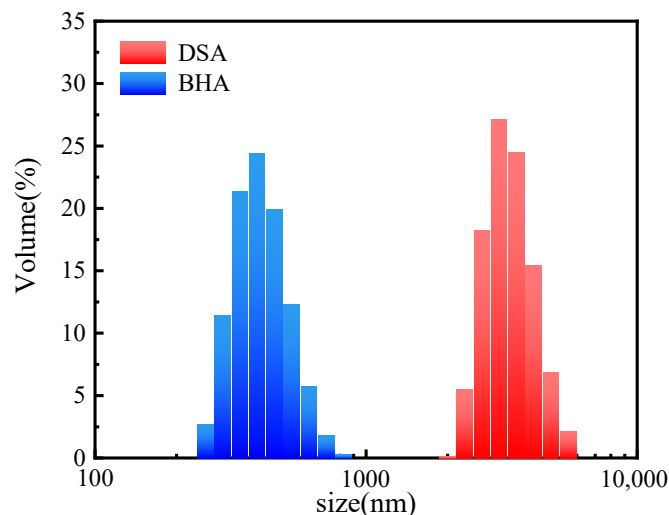


**Figure 9.** Size distribution of DSA and BHA molecular clusters.

### 3.2.5. Discussion of Adsorption Models

The adsorption mechanisms of DSA and BHA on the surface of cassiterite were investigated through zeta potential, FTIR, and XPS analyses. These results collectively suggest that the adsorption of DSA onto cassiterite is a result of a synergistic effect involving both electrostatic and chemical interactions. Specifically, the nitrogen (N) or oxygen (O) atoms present in the DSA molecule play a crucial role in binding to the tin (Sn) sites on the cassiterite surface. This interaction leads to the formation of stable chelating rings, which is a mechanism akin to the adsorption process observed for BHA on cassiterite surfaces [24]. Additionally, the findings from cluster size measurements reveal a significant difference in the hydrophobicity between DSA and BHA. DSA exhibits a notably higher degree of hydrophobicity compared to BHA, and this characteristic contributes to its larger effective adsorption capacity on the cassiterite surface. In summary, DSA demonstrates a superior recovery effect on cassiterite compared to BHA, and this effect can be achieved at a lower dosage. For a visual representation of this adsorption process, please refer to Figure 10, which presents a simplified adsorption model illustrating how DSA and BHA interact with the cassiterite surface.

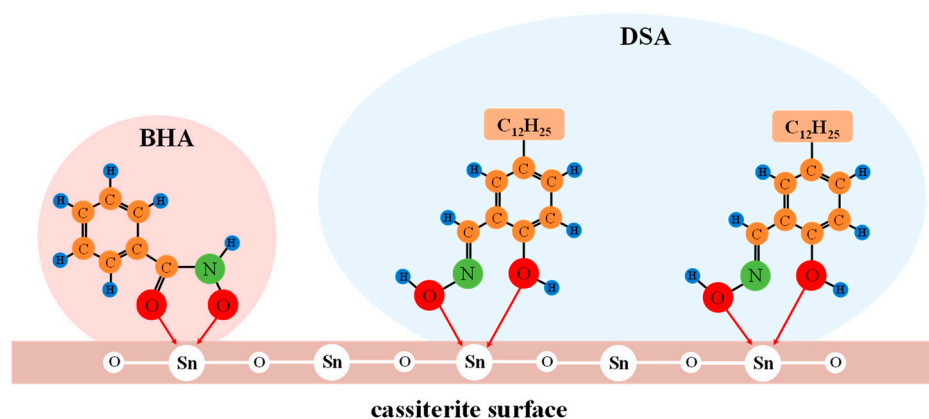


**Figure 10.** Adsorption model of DSA and BHA on the cassiterite surface.

### 3.3. Production Application

Bench-scale flotation tests were conducted to evaluate the recovery efficiency of DSA on cassiterite within a challenging slurry environment. These experiments utilized a copper–tin polymetallic ore sourced from Yunnan Province, China. The ore samples contain valuable minerals such as cassiterite, pyrite, and hematite. Meanwhile, the primary

gangue minerals present in the ore include quartz, magnesium tourmaline, and mica, as well as trace amounts of microcline and chlorite. The XRD spectrum of the ore sample is shown in Figure 11. The elemental composition of the raw ore is provided in Table 1.

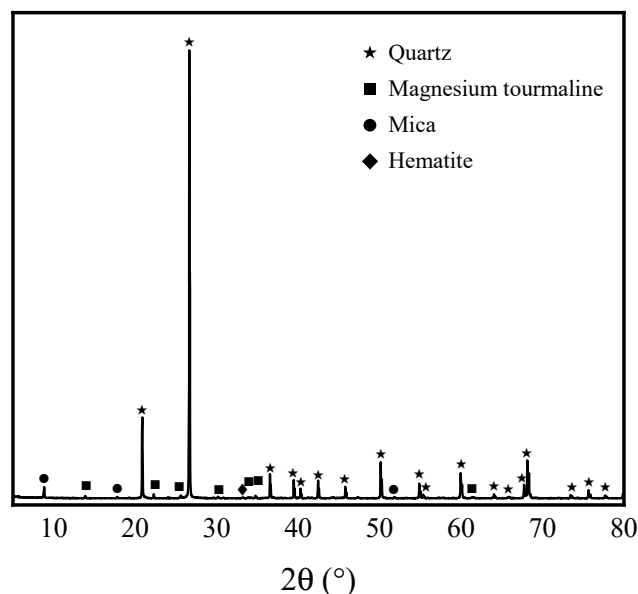


Figure 11. XRD pattern of ore samples.

Table 1. Chemical composition of raw ore (wt %).

Elements	Sn	Fe	O	Si	Ca	Al	Mg	Else
Content (wt %)	0.481	2.593	51.00	41.12	0.24	1.76	1.14	1.6657

Based on the initial single-factor open-circuit experiment, a closed-circuit flotation experiment was performed. The beneficiation process and reagent system for the ore are shown in Figure 12. The results of closed-circuit flotation tests using DSA and BHA as collectors are shown in Table 2.

Table 2. The results of closed-circuit flotation tests (wt %).

Conditions	Products	Yield	Sn Grade	Sn Recovery
DSA	Concentrate	2.55	14.751	78.20
	Tailings	97.45	0.108	21.80
	Raw ore	100	0.480	100
BHA	Concentrate	2.11	15.026	65.91
	Tailings	97.89	0.167	34.09
	Raw ore	100	0.481	100

The DSA still exhibits excellent selectivity and collectivity in actual ore flotation. The recovery rate is as high as 78.20% when the Sn grade remains essentially constant, which is 12.29% higher than that of the BHA as a collector and potentially of application value.

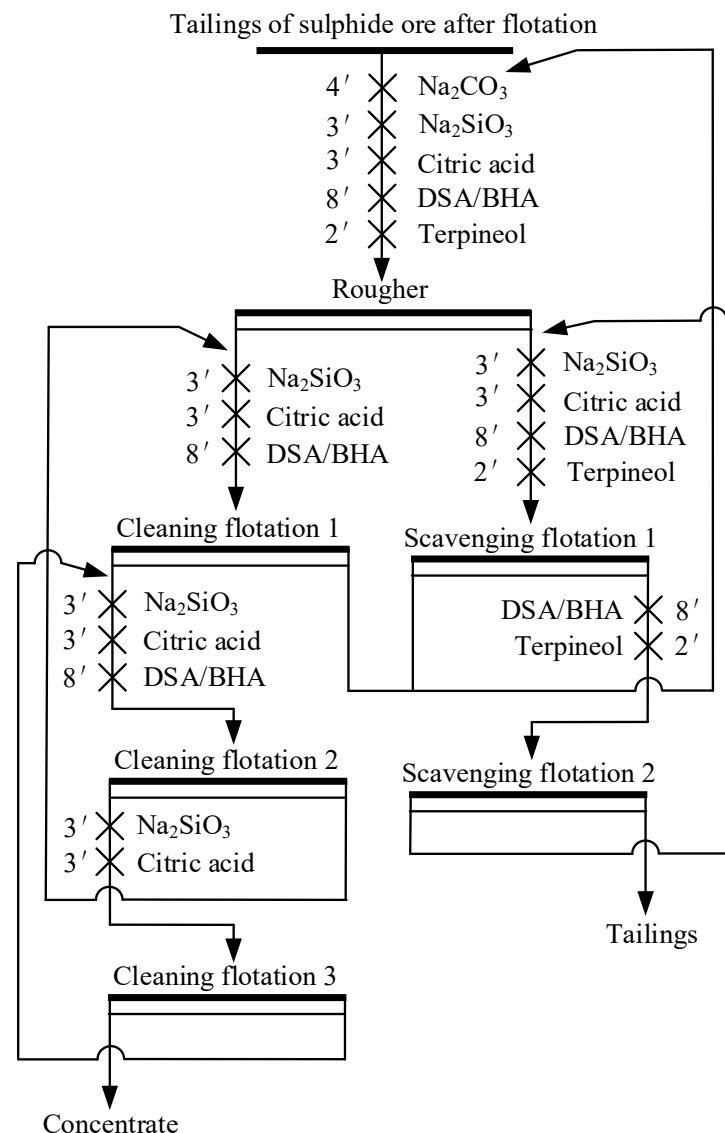


**Figure 12.** The flowsheet of the bench-scale flotation tests.

#### 4. Conclusions

5-dodecylsalicylaldoxime (DSA) has emerged as an exceptional flotation collector for cassiterite, displaying outstanding selectivity and effectiveness. To shed light on the adsorption mechanism of DSA onto the cassiterite surface, a series of tests, including zeta potential analysis, FTIR, and XPS, were conducted. The reasons behind DSA's superior recovery performance compared to BHA were elucidated through measurements of reagent molecular cluster size. The main results are summarized as follows:

- (1) In the micro-flotation test, the recovery of cassiterite reached an impressive 82.5% at a concentration of  $9 \times 10^{-5}$  mol/L, without the need for any activator. In the micro-flotation test of artificially mixed minerals, the concentrate with a Sn grade of 24.98% and a recovery of 80.44% was obtained at the same reagent concentration. Compared to BHA, while the Sn grade is similar, DSA achieved a 33.55% higher recovery.
- (2) Findings from zeta potential tests, FTIR, and XPS analyses indicate that DSA forms a stable chelating ring with the cassiterite surface, facilitated by the N and O atoms within its CH=NOH and C-OH groups. This adsorption mechanism resembles the process observed for BHA on cassiterite surfaces.

- (3) Analysis of reagent molecular cluster sizes reveals that DSA forms larger molecular clusters in the pulp and exhibits higher hydrophobicity than BHA. At equivalent active sites, DSA had a larger effective adsorption capacity than BHA, leading to enhanced hydrophobicity on the cassiterite surface and, thereby, favoring flotation recovery.
- (4) In a closed-circuit test of cassiterite flotation recovery in a copper–tin polymetallic ore in Yunnan, DSA achieved impressive results. It yielded a concentrate with a Sn grade of 14.751% and a recovery of 78.20% from raw ore with a Sn grade of 0.481%. Notably, this recovery surpassed that achieved with BHA as a collector by 12.29% while maintaining a nearly identical grade.

**Author Contributions:** Formal analysis, visualization, investigation, writing—original draft, L.S. and Y.Q.; formal analysis, data curation, investigation, writing—review and editing, Y.C. and Q.W.; investigation, data curation, formal analysis, X.W.; methodology, project administration, resources, funding acquisition, supervision, writing—review and editing, G.L.; conceptualization, methodology, funding acquisition, W.S. All authors have read and agreed to the published version of the manuscript.

**Funding:** The authors would like to sincerely thank the National Key Research and Development Program of China (2023YFC3904202), Major Science and Technology Program of Yunnan Province China (202202AB080012), supported by the Fundamental Research Funds for the Central Universities of Central South University (CX20230212).

**Data Availability Statement:** Data that support the findings of this study are available from the corresponding author upon reasonable request due to privacy.

**Acknowledgments:** We sincerely thank the academic editors and anonymous reviewers for their constructive comments.

**Conflicts of Interest:** The authors declare no conflicts of interest.

## References

1. Amosah, M.; Yvon, M.; Zhou, J.; Galvin, K. The role of enhanced desliming and gravity separation as a precursor to flotation in the upgrading of cassiterite from tailings. *Miner. Eng.* **2024**, *208*, 108581. [[CrossRef](#)]
2. Yang, C.; Tan, Q.; Zeng, X.; Zhang, Y.; Wang, Z.; Li, J. Measuring the sustainability of tin in China. *Sci. Total Environ.* **2018**, *635*, 1351–1359. [[CrossRef](#)] [[PubMed](#)]
3. Kempf, A.; Kiefer, S.; Graczyk-Zajac, M.; Ionescu, E.; Riedel, R. Tin-functionalized silicon oxycarbide as a stable, high-capacity anode material for Na-ion batteries. *Open Ceram.* **2023**, *15*, 100388. [[CrossRef](#)]
4. Izard, C.F.; Müller, D.B. Tracking the devil’s metal: Historical global and contemporary U.S. tin cycles. *Resour. Conserv. Recycl.* **2010**, *54*, 1436–1441. [[CrossRef](#)]
5. Su, Z.; Zhang, Y.; Liu, B.; Lu, M.; Li, G.; Jiang, T. Extraction and Separation of Tin from Tin-Bearing Secondary Resources: A Review. *JOM* **2017**, *69*, 2364–2372. [[CrossRef](#)]
6. Clauss, C.R.A.; Appleton, E.A.; Vink, J.J. Selective flocculation of cassiterite in mixtures with quartz using a modified polyacrylamide flocculant. *Int. J. Miner. Process.* **1976**, *3*, 27–34. [[CrossRef](#)]
7. Angadi, S.I.; Eswaraiyah, C.; Jeon, H.-S.; Mishra, B.K.; Miller, J.D. Selection of Gravity Separators for the Beneficiation of the Uljin Tin Ore. *Miner. Process. Extr. Metall. Rev.* **2017**, *38*, 54–61. [[CrossRef](#)]
8. Zhang, L.; Khoso, S.; Tian, M.; Sun, W. Cassiterite recovery from a sulfide ore flotation tailing by combined gravity and flotation separations. *Physicochem. Probl. Miner. Process.* **2020**, *57*, 206–215. [[CrossRef](#)]
9. Angadi, S.I.; Sreenivas, T.; Jeon, H.-S.; Baek, S.-H.; Mishra, B.K. A review of cassiterite beneficiation fundamentals and plant practices. *Miner. Eng.* **2015**, *70*, 178–200. [[CrossRef](#)]
10. Leistner, T.; Embrechts, M.; Leißner, T.; Chehreh Chelgani, S.; Osbahr, I.; Möckel, R.; Peuker, U.A.; Rudolph, M. A study of the reprocessing of fine and ultrafine cassiterite from gravity tailing residues by using various flotation techniques. *Miner. Eng.* **2016**, *96–97*, 94–98. [[CrossRef](#)]
11. Wang, X.; Liu, J.; Zhu, Y.; Li, Y. Adsorption and depression mechanism of an eco-friendly depressant PBTCa on fluorite surface for the efficient separation of cassiterite from fluorite. *Miner. Eng.* **2021**, *171*, 107124. [[CrossRef](#)]
12. Peng, H.; Luo, W.; Wu, D.; Bie, X.; Shao, H.; Jiao, W.; Liu, Y. Study on the Effect of Fe<sup>3+</sup> on Zircon Flotation Separation from Cassiterite Using Sodium Oleate as Collector. *Minerals* **2017**, *7*, 108. [[CrossRef](#)]
13. Gruner, H.; Bilsing, U. Cassiterite flotation using styrene phosphonic acid to produce high-grade concentrates at high recoveries from finely disseminated ores—comparison with other collectors and discussion of effective circuit configurations. *Miner. Eng.* **1992**, *5*, 429–434. [[CrossRef](#)]

14. Ren, L.; Zhang, Z.; Zeng, W.; Zhang, Y. Adhesion between nanobubbles and fine cassiterite particles. *Int. J. Min. Sci. Technol.* **2023**, *33*, 503–509. [[CrossRef](#)]
15. Ren, L.; Zhang, Y.; Qin, W.; Bao, S.; Wang, J. Collision and attachment behavior between fine cassiterite particles and H<sub>2</sub> bubbles. *Trans. Nonferrous Met. Soc. China* **2014**, *24*, 520–527. [[CrossRef](#)]
16. Chen, Y.; Tong, X.; Feng, D.; Xie, X. Effect of Al (III) Ions on the Separation of Cassiterite and Clinocllore Through Reverse Flotation. *Minerals* **2018**, *8*, 347. [[CrossRef](#)]
17. Xu, Y.; Qin, W. Surface Analysis of Cassiterite with Sodium Oleate in Aqueous Solution. *Sep. Sci. Technol.* **2012**, *47*, 502–506. [[CrossRef](#)]
18. Abaka-Wood, G.B.; Addai-Mensah, J.; Skinner, W. Selective flotation of rare earth oxides from hematite and quartz mixtures using oleic acid as a collector. *Int. J. Miner. Process.* **2017**, *169*, 60–69. [[CrossRef](#)]
19. Ding, Z.; Li, J.; Yuan, J.; Yu, A.; Wen, S.; Bai, S. Insights into the influence of calcium ions on the adsorption behavior of sodium oleate and its response to flotation of quartz: FT-IR, XPS and AMF studies. *Miner. Eng.* **2023**, *204*, 108437. [[CrossRef](#)]
20. Pei, B.; Li, J.; Liu, Z.; Ning, S.; Cai, Z.; Liu, R. Reverse flotation separation of calcite/dolomite from hemimorphite based on their surface sulphophile and oxyphile affinity differences. *Colloids Surf. A* **2024**, *682*, 132932. [[CrossRef](#)]
21. Liu, J.; Kong, D.; Xie, R.; Li, Y.; Zhu, Y.; Liu, C. Flotation behavior and mechanism of hydroxycitric acid as a depressant on the flotation separation of cassiterite from calcite. *Miner. Eng.* **2021**, *170*, 107046. [[CrossRef](#)]
22. Li, F.; Zhong, H.; Zhao, G.; Wang, S.; Liu, G. Flotation performances and adsorption mechanism of  $\alpha$ -hydroxyoctyl phosphinic acid to cassiterite. *Appl. Surf. Sci.* **2015**, *353*, 856–864. [[CrossRef](#)]
23. Lu, Y.; Wang, S.; Zhong, H. Optimization of conventional hydroxamic acid for cassiterite flotation: Application of structural modification under principle of isomerism. *Miner. Eng.* **2021**, *167*, 106901. [[CrossRef](#)]
24. Sun, L.; Hu, Y.; Sun, W. Effect and mechanism of octanol in cassiterite flotation using benzohydroxamic acid as collector. *Trans. Nonferrous Met. Soc. China* **2016**, *26*, 3253–3257. [[CrossRef](#)]
25. Wu, X.; Zhu, J. Selective flotation of cassiterite with benzohydroxamic acid. *Miner. Eng.* **2006**, *19*, 1410–1417. [[CrossRef](#)]
26. Qin, W.; Xu, Y.; Liu, H.; Ren, L.; Yang, C. Flotation and Surface Behavior of Cassiterite with Salicylhydroxamic Acid. *Ind. Eng. Chem. Res.* **2011**, *50*, 10778–10783. [[CrossRef](#)]
27. Cai, J.; Wu, B.; Deng, J.; Hu, M.; Wu, M.; Wei, P.; Sun, X.; Qiu, H.; Jin, X.; Hou, X.; et al. A novel approach to improve cassiterite recovery based on grinding. *Powder Technol.* **2022**, *400*, 117257. [[CrossRef](#)]
28. Agrawal, Y.K.; Tandon, S.G. Solution stability constants of complexes of benzohydroxamic acid with some divalent metal ions. *J. Inorg. Nucl. Chem.* **1972**, *34*, 1291–1295. [[CrossRef](#)]
29. Fu, J.; Han, H.; Wei, Z.; Liu, R.; Li, W.; Xu, T.; Ji, D. Selective separation of scheelite from calcite using tartaric acid and Pb-BHA complexes. *Colloids Surf. A* **2021**, *622*, 126657. [[CrossRef](#)]
30. Sreenivas, T.; Padmanabhan, N.P.H. Surface chemistry and flotation of cassiterite with alkyl hydroxamates. *Colloids Surf. A* **2002**, *205*, 47–59. [[CrossRef](#)]
31. Jin, S.; Zhang, P.; Ou, L.; Zhang, Y.; Chen, J. Flotation of cassiterite using alkyl hydroxamates with different carbon chain lengths: A theoretical and experimental study. *Miner. Eng.* **2021**, *170*, 107025. [[CrossRef](#)]
32. Houchin, M.R.; Warren, L.J. Surface titrations and electrokinetic measurements on Australian cassiterites. *Colloids Surf.* **1985**, *16*, 117–126. [[CrossRef](#)]
33. Balachandran, S.B.; Simkovich, G.; Aplan, F.F. The influence of point defects on the floatability of cassiterite, I. Properties of synthetic and natural cassiterites. *Int. J. Miner. Process.* **1987**, *21*, 157–171. [[CrossRef](#)]
34. Stachurski, J.; Michalek, M. The Effect of the  $\zeta$  Potential on the Stability of a Non-Polar Oil-in-Water Emulsion. *J. Colloid Interface Sci.* **1996**, *184*, 433–436. [[CrossRef](#)]
35. Zhu, L.; Liu, J.; Zhu, Y.; Gong, G.; Han, Y. Mechanism of HCA and CEPPA in flotation separation of cassiterite and fluorite. *Miner. Eng.* **2022**, *187*, 107773. [[CrossRef](#)]
36. Losos, Z.; Beran, A. OH defects in cassiterite. *Mineral. Petrol.* **2004**, *81*, 219–234. [[CrossRef](#)]
37. Zheng, Z.P.; Fan, W.H.; Yan, H.; Liu, J.; Yang, W.Z.; Zhu, S.L. Terahertz and mid-infrared spectroscopy of benzene-1,2-diol. *J. Mol. Spectrosc.* **2012**, *281*, 13–17. [[CrossRef](#)]
38. Keefe, C.D.; Gillis, E.A.L. Temperature dependence of the optical properties of liquid benzene in the infrared between 25 and 50 °C. *Spectrochim. Acta Part A* **2008**, *70*, 500–509. [[CrossRef](#)] [[PubMed](#)]
39. Li, J.; Nie, G.; Li, J.; Zhu, Z.; Wang, Z. Flotation separation of quartz and dolomite from colophane using sodium N-dodecyl- $\beta$ -amino propionate and its adsorption mechanism. *Colloids Surf. A* **2022**, *641*, 128586. [[CrossRef](#)]
40. Xu, H.; Zhong, H.; Wang, S.; Niu, Y.; Liu, G. Synthesis of 2-ethyl-2-hexenal oxime and its flotation performance for copper ore. *Miner. Eng.* **2014**, *66–68*, 173–180. [[CrossRef](#)]
41. Morozov, I.G.; Belousova, O.V.; Blanco-Andujar, C.; Ortega, D.; Kuznetsov, M.V. Structural, optical, magnetic, and XPS properties of SnOx nanoparticles. *Solid State Sci.* **2022**, *126*, 106854. [[CrossRef](#)]
42. Cao, Y.; Sun, L.; Gao, Z.; Sun, W.; Cao, X. Activation mechanism of zinc ions in cassiterite flotation with benzohydroxamic acid as a collector. *Miner. Eng.* **2020**, *156*, 106523. [[CrossRef](#)]
43. Feng, Q.; Zhao, W.; Wen, S.; Cao, Q. Activation mechanism of lead ions in cassiterite flotation with salicylhydroxamic acid as collector. *Sep. Purif. Technol.* **2017**, *178*, 193–199. [[CrossRef](#)]

44. Wang, Q.; Sun, L.; Cao, Y.; Wang, X.; Qiao, Y.; Liu, G.; Xiang, M.; Sun, W. Flotation Separation of Smithsonite from Calcite Using Cupferron as a Collector. *Minerals* **2023**, *13*, 992. [[CrossRef](#)]
45. Tian, M.; Liu, R.; Gao, Z.; Chen, P.; Han, H.; Wang, L.; Zhang, C.; Sun, W.; Hu, Y. Activation mechanism of Fe (III) ions in cassiterite flotation with benzohydroxamic acid collector. *Miner. Eng.* **2018**, *119*, 31–37. [[CrossRef](#)]

**Disclaimer/Publisher’s Note:** The statements, opinions and data contained in all publications are solely those of the individual author(s) and contributor(s) and not of MDPI and/or the editor(s). MDPI and/or the editor(s) disclaim responsibility for any injury to people or property resulting from any ideas, methods, instructions or products referred to in the content.